Weierstraß-Institut
für Angewandte Analysis und Stochastik
Leibniz-Institut im Forschungsverbund Berlin e. V.

Preprint ISSN 0946 – 8633

Spectral delay algebraic equation approach to broad area laser diodes

Antonio Pérez-Serrano[1], Julien Javaloyes[2] , Salvador Balle[3]

submitted: December 18, 2012

[1] Weierstrass Institute
Mohrenstr. 39
10117 Berlin
Germany
E-Mail: Antonio.Perez-Serrano@wias-berlin.de

[2] Universitat de les Illes Balears
Cra. Valldemossa, km 7.5
07122 Palma de Mallorca
Spain
E-Mail: julien.javaloyes@uib.es

[3] Institut Mediterrani d'Estudis Avançats
C/ Miquel Marquès 21
07190 Esporles
Spain
E-Mail: salvador@imedea.uib-csic.es

No. 1755
Berlin 2012

2010 *Mathematics Subject Classification.* 78A60, 65P99, 65M70, 65Y20.

2010 *Physics and Astronomy Classification Scheme.* 42.55.Px, 42.60.Jf, 42.60.Mi, 42.65.Sf.

Key words and phrases. Semiconductor lasers, broad area laser diode (BALD), traveling wave model (TWM).

The authors acknowledge fruitful discussions with M. Radziunas, H. Wenzel and U. Bandelow.
J.J. acknowledges financial support from the Ramon y Cajal fellowship. J.J. and S.B. acknowledge financial support from project RANGER (TEC2012-38864-C03-01) and from the Direcció General de Recerca, Desenvolupament Tecnològic i Innovació de la Conselleria d'Innovació, Interior i Justícia del Govern de les Illes Balears co-funded by the European Union FEDER funds.

Edited by
Weierstraß-Institut für Angewandte Analysis und Stochastik (WIAS)
Leibniz-Institut im Forschungsverbund Berlin e. V.
Mohrenstraße 39
10117 Berlin
Germany

Fax: +49 30 20372-303
E-Mail: preprint@wias-berlin.de
World Wide Web: http://www.wias-berlin.de/

Abstract

In this work, we discuss an efficient modeling approach for the simulation of Broad Area Laser Diodes. Our method is based on the analytical solution in the spectral domain of the paraxial wave equations for the forward and backward slowly varying traveling waves. We show how to extend to the lateral dimension and to the influence of diffractive terms the idea of mesh decimation by recasting traveling wave models into coupled delay algebraic equations, as discussed in [1]. We compare the results of the dynamics obtained with our improved model with the results of a standard traveling wave description in the cases of straight current stripes as well as in the important configuration of high power tapered anti-reflection coated devices. We obtain an excellent agreement and an improvement of the integration time between one and two orders of magnitudes which may alleviate the necessity of using complex parallel codes. We discussed how the method can be further improved to other, more refined descriptions of the active medium and to the inclusion of thermal effects.

1 Introduction

The optical power that can be extracted from a Semiconductor Laser (SL) is limited because of Catastrophic Optical Damage (COD). One path used to circumvent this limit is to increase the volume of the lasing mode, which in the simplest case is achieved by increasing the lateral dimension, thus leading to the so-called Broad-Area Laser Diodes (BALDs). BALDs are usually easy to fabricate which makes these devices useful for characterizing the properties of the active material because parameters like the gain, the differential gain and the quantum efficiency can be extracted from their L-I curve. Typical BALDs have lateral dimensions of the order of $100\ \mu$m - $500\ \mu$m, and allow to obtain CW output powers of the order of 10 W [2]. However, the emission profile of these lasers usually presents a low quality, with M^2 factors substantially larger than unity [3], which prevents their application in fields where a close to diffraction limited beam is required, such as for example marking. As a consequence, BALDs are mainly used for optical pumping of high-power solid-state lasers, and specialized optical manipulation of their beam is required for pumping of fiber amplifiers or lasers [4].

The poor beam quality of BALDs originates from their large lateral dimension, which allows for many lateral modes that are nearly degenerated in gain. This leads to multipeaked near-fields, but more important, the spatial profile usually depends on the current value due to carrier-induced self-focusing, which might even lead to chaotic filamentation of the beam [5]. The origin of this phenomenon is the so-called Spatial Hole Burning (SHB): in regions of high optical intensity, the local gain (and thus the local carrier density) is depressed by stimulated emission; this depression leads to a local increase of refractive index which tends to further confine the

light and to increase the local field intensity. An additional consequence of filamentation is that the resulting SHB leads to multimode operation.

Several strategies have been proposed to improve beam quality in BALDs, mostly based on spatial filtering aimed at suppressing higher order lateral modes, e.g. the use of Bragg gratings [6], the α-DFB [7, 8], unstable resonators [9, 10], optical feedback [11, 12], tapered lasers [13], master-oscillator/power amplifiers (MOPAs) [14] or etched patterns [15]. However, filamentation due to SHB depends on the working point of the laser and its analysis requires models and simulation tools that take into account the whole state of the system. Different physical models have been proposed in order to understand the behavior and the modal properties of BALDs. These models are based mainly in the paraxial wave-equation completed with the Bloch equation for the carriers and the induced polarization of the medium, but there are other approaches based on stationary electro-thermal-optical characteristics [16]. A traditional used approach to numerically compute the stationary solutions of these approaches are based on Beam Propagation Methods (BPMs), specially the Fox and Li method [17] using Perfectly Matched Layer (PML) boundary conditions [18]. Other stationary approaches to calculate the modes of BALDs are based in resulting Helmholtz equations from performing the mean-field approximation in the longitudinal direction [19] and performing the Linear Stability Analysis (LSA) via a Green function method [20].

However, a time-dependent approach would be the appropriate choice in order to assess multimode behavior and filamentation effects. Such approaches have been successfully applied to BALDs, amplifiers and tapered lasers. They are based on discretized schemes like for example the Hopscotch method [21], an explicit scheme with some implicit character, or split traveling-wave models (TWMs) where the diffraction in the lateral dimension is computed via spectral methods [14]. From the numerical point of view, the two-dimensional character of the field and of the carrier distributions combined with the large spectral width ($\sim 10 - 50$ nm) of the gain curve in semiconductor materials, result in models that are characterized by huge number of degrees of freedom (DOF). Such large numbers of DOF demand an exceedingly large computing power for performing exhaustive simulations in the asymptotic regimes using standard Finite-Differences Time-Domain (FDTD) approaches [22]. In general, all the spatially resolved and time dependent approaches are strongly hindered by the stiffness of laser dynamics: to properly account for the broad gain spectrum one must use an appropriately small time step δt, while the Courant-Friedrichs-Lewy (CFL) [23] condition for numerical stability imposes an accordingly fine spatial discretization δz.

Recently, it was shown by some of us [1] that a one dimensional TWM can be recast into an ensemble of a few coupled Delayed Algebraic Equation. The method relies on approximating the analytic solution of the field propagation equation, and allows to substantially reduce the number of DOF that must be non trivially updated after each time step, as compared to methods based on finite-differences. It was shown in [1] that such a description for a bi-directionaly emitting laser cavity containing an extended medium permits to drastically reduce the computation time as compared to a TWM while accurately preserving the dynamics even in the strongly non linear regimes of passive mode-locking. The large reduction in complexity allowed for a direct linear stability analysis (LSA) and numerical bifurcation diagram reconstruction. However the method discussed in [1] cannot be applied *per se* in the case of a multi-dimensional laser due to the

presence of diffraction in the transverse plane that must be properly accounted for.

In this paper we present an efficient model for the simulation of BALDs that is based on a combination of a Fourier method and of the Delay Algebraic Equations method developed for the simulation of narrow-stripe SLs [1]. The resulting model consists in several coupled DAEs in the Fourier domains describing the temporal evolution of the optical field that are coupled to the active medium polarization that is still described in the direct space.

The article is organized as follow: In section II, we detail outline our modeling approach and the numerical method we developed. In Section III, we explain the major results of the decimation method and how it allows to recover known results of the dynamics of BALDs like the so called zipper states and the transition to chaotic transverse and longitudinal dynamics. We also discuss the important case of the dynamics of tapered laser. The conclusions are given in Section IV.

2 Model

2.1 Traveling-Wave equations

Our model for the gain-guided BALD considers a single polarization mode in the transverse direction. The optical field in the cavity is assumed to be almost TE polarized and it is decomposed into a forward and a backward wave, $E_{\pm}(x,z,t)$, whose instantaneous distributions in the lateral (x) and longitudinal (z) direction are described in the paraxial approximation by a TWM [24] extended to include diffraction in the transverse dimension. In addition, the carrier density $N(x,z,t)$ in the cavity is decomposed into a quasi-homogeneous term $N_0(x,z,t)$ and a grating term at half the optical wavelength, $N_{\pm 2}(x,z,t)$, with $N_{-2}(x,z,t) = N_2^*(x,z,t)$. Scaling the two spatial coordinates and time as $(x,z,t) = (X,Z,T)/(L_x,L_z,\tau)$, where the time of flight in the cavity is $\tau = nL_z/c$, the resulting equations read

$$\begin{aligned}
\left(\partial_t \pm \partial_z\right) E_{\pm} &= i\Delta\partial_x^2 E - \alpha_i E_{\pm} + iP_{\pm}\,, && (1)\\
\partial_t N_0 &= J\left(x,z\right) - R\left(N_0\right) + \mathcal{D}\partial_x^2 N_0 - i\left(P_+E_+^{\star} + P_-E_-^{\star} - c.c.\right), && (2)\\
\partial_t N_{\pm 2} &= -\left(R'\left(N_0\right) + 4\mathcal{D}q^2\right) N_{\pm 2} - i\left(P_{\pm}E_{\mp}^{\star} - E_{\pm}P_{\mp}^{\star}\right), && (3)\\
R\left(N\right) &= AN + BN^2 + CN^3. && (4)
\end{aligned}$$

where α_i takes into account for the internal losses, $J(x,y)$ is the space dependent pump current, $\mathcal{D} = \tilde{\mathcal{D}}L_x^{-2}$ is the scaled diffusion length and $\Delta = \lambda_0/(4\pi n)L_zL_x^{-2}$ is the scaled diffraction length, with λ_0 the wavelength in vacuum and n is the group index. For the sake of simplicity we have neglected the transverse diffusion (i.e. $\mathcal{D}\partial_x^2 N_2$) of the longitudinal population grating N_2 since the actual decay rate $4\mathcal{D}q^2 \sim 10^{12}\,\mathrm{s}^{-1}$ correspond to a length well below the diffusion length. The carriers are normalized to the transparency density N_t and the non linear recombination $R\left(N\right)$ contains the non radiative (A), the radiative (B) and the Auger (C) contributions. The boundary conditions at the left and right facets reads in the simplest case of a Fabry-Pérot cavity

$$\begin{aligned}
E_+\left(x,0,t\right) &= r_l E_-\left(x,0,t\right),\\
E_-\left(x,1,t\right) &= r_r E_+\left(x,1,t\right).
\end{aligned} \qquad (5)$$

The field amplitudes and the carrier density components are coupled through the polarizations of the active medium, $P_{\pm}(x,z,t)$, which describe in time-domain the carrier-induced gain and refractive index experienced by the forward and backward fields. Analytical approximations to the optical response of the medium in frequency-domain exist in simplified cases (two parabolic bands and assuming low temperature) either including [25] or not [26] spectral hole burning in the carrier distribution. When spectral hole burning is negligible, a time-domain description of the material polarization $P(x,z,t)$ can be found in the intraband quasi-equilibrium approximation, which is valid for time scales longer than the intraband relaxation rates (~ 0.1 ps) [27]. In this limit, $P(x,z,t)$ is described by a convolution kernel that reproduces the full gain curve of the semiconductor material hence permitting to describe both gain and absorbing sections simultaneously. When the dynamics is restricted to the vicinity of the band-gap, as is the case of BALDs, it is possible to use a simpler Padé approximation to the optical response as that developed in [28].

In the asymptotic limit of a very broad semiconductor band (i.e. $b \to \infty$ with the notations of [26]), the link between the polarization and the field is given in frequency domain as

$$P(x,z,\omega) = \chi\left[D(x,z),\omega\right] E(x,z,\omega), \tag{6}$$

$$\chi(D,\omega)/\chi_0 = \ln\left(\frac{\omega}{\gamma}+i\right) - 2\ln\left(\frac{\omega}{\gamma}+i-D\right) + i\pi + \ln 2, \tag{7}$$

where $D(x,z) = N(x,z)/N_t$ denotes the carrier density at point (x,z) normalized to the transparency carrier density. The gain, given by the imaginary part of χ, has a maximum at frequency $\omega_p(D) = \gamma\left(\sqrt{2D^2-1}-D\right)$. A diagonal Padé[1,1] approximation of the frequency domain susceptibility around the dynamic frequency ω_p where the gain is maximal reads

$$\chi(D,\omega) \simeq \frac{\chi(D,\omega_p)+(\omega-\omega_p)\,a}{1+(\omega-\omega_p)\,b}, \tag{8}$$

$$a = \chi(D,\omega_p)\,b + \partial_\omega\chi(D,\omega_p), \tag{9}$$

$$b = -\frac{1}{2}\frac{\partial^2_\omega\chi(D,\omega_p)}{\partial_\omega\chi(D,\omega_p)}, \tag{10}$$

The polarization at a given point (x,z) therefore reads

$$\left[1+(\omega-\omega_p)\,b(x,z)\right] P(x,z,\omega) = \left[\chi\left[D(x,z),\omega_p\right]+(\omega-\omega_p)\,a(x,z)\right] E(x,z,\omega), \tag{11}$$

where the spatial dependence of a and b arises from that of D. In the cases where the gain does no possess a maxima, as for instance in the unpumped regions around the gain stripe, the Padé approximation is performed at the band-gap frequency, i.e. $\omega_p = 0$.

Decomposing the field into forward and backward waves and the carrier density into homogeneous and grating terms, and assuming the grating term to be small in comparison to the homogeneous one, we find that

$$
\begin{aligned}
\left[1+\left(\omega-\omega_p\right)b\left(x,z\right)\right]P_{\pm}\left(x,z,\omega\right) &= \\
\left[\chi\left[D_0\left(x,z\right),\omega_p\right]+\left(\omega-\omega_p\right)a\left(x,z\right)\right]E_{\pm}\left(x,z,\omega\right) &+ \\
\partial_D\chi\left(D_0(x,z),\omega_p\right)D_{\pm 2}(x,z)E_{\mp}(x,z,\omega) &\quad , \qquad (12)
\end{aligned}
$$

where we have neglected the impact of the grating terms on a and b. Finally, using that $\partial_t \rightarrow -i\omega$, the time domain evolution equation for the polarizations can be written as

$$
\partial_t P_{\pm} = -\left(\frac{1}{ib}+i\omega_p\right)P_{\pm}+\frac{\chi-\omega_p a}{ib}E_{\pm}+\frac{a}{b}\partial_t E_{\pm}+\frac{\partial_D\chi}{ib}D_{\pm 2}E_{\mp}, \qquad (13)
$$

where $\chi=\chi(D_0(x,z,t),\omega_p)$ and a and b are given by eq. (9) and eq. (10), respectively, with $D=D_0(x,z,t)$.

2.2 Numerical method

Our numerical method for solving eqs. (1-4) and eq. (13) adapts the Delay Algebraic Equation (DAE) approach developed in [1] to the case of a gain guided BALD. The main difficulty arises from the diffractive term in eq. (1) as any approximation over the spatial derivative using e.g. finite differences would introduce numerical artifacts in the dispersion relation of the transverse mode and therefore potentially spoils the dynamics. This problem can be circumvented by Fourier transforming eq. (1) along x which leads again to an uni-dimensional TWM. This allows to exploit the exact solution by integrating over the so-called forward and backward characteristics [29] and to obtain again a DAE that reads

$$
E_{\pm}\left(q,z,t\right)=E_{\pm}\left(q,z\mp h,t-h\right)e^{-\left(i\Delta q^2+\alpha_i\right)h}+i\mathcal{S}_{\pm}, \qquad (14)
$$

$$
\mathcal{S}_{\pm} = \int_0^h dsP_{\pm}\left(q,z\mp s,t-s\right)e^{\left(i\Delta q^2+\alpha_i\right)s}. \qquad (15)
$$

The source term $\mathcal{S}_{\pm}$ is approximated by assuming a linear variation of the polarization in Fourier space along the characteristics, i.e. we assume that the distance h between the two points is short enough for the Uniform Field Limit (UFL) to hold and as such we have that

$$
\mathcal{S}_{\pm} \simeq w_1 P_{\pm}\left(q,z\mp h,t-h\right)+w_2\left[P_{\pm}\left(q,z,t\right)-P_{\pm}\left(q,z\mp h,t-h\right)\right], \qquad (16)
$$

$$
w_1 = \frac{e^{\left(i\Delta q^2+\alpha_i\right)h}-1}{\left(i\Delta q^2+\alpha_i\right)}, \qquad (17)
$$

$$
w_2 = \frac{e^{\left(i\Delta q^2+\alpha_i\right)h}\left[\left(i\Delta q^2+\alpha_i\right)h-1\right]+1}{\left(i\Delta q^2+\alpha_i\right)^2 h}. \qquad (18)
$$

The approximation in eq. (16) is valid up to second order in h, the length of the characteristics. Notice also that in eqs. (14,15) the treatment of propagation losses and of diffraction is exact.

Hence the full modal structure of the resonator is perfectly reproduced. One remarks that such a DAE can be written only in Fourier space which is not convenient for the active material description. Hence the methodology consists in transforming back in forth between the direct and the Fourier space to update the field and the polarization and carriers with the following sequence (fields in Fourier and direct space are denoted by the same letters but depend either on x or on q):

1 Perform a first order explicit Euler prediction of $E_{\pm}\left(q, z, t+\delta t\right)$ and transform back to space (x) domain to obtain a first order estimate of $E_{\pm}\left(x, z, t+\delta t\right)$.

2 Perform a second order semi-implicit evolution of the polarization and get $P_{\pm}\left(x, z, t+\delta t\right)$ as in [28] and Fourier transform to get $P_{\pm}\left(q, z, t+\delta t\right)$.

3 Perform the second order semi-implicit evaluation of $E_{\pm}\left(q, z, t+\delta t\right)$ as in [28] and transform back to space (x) domain to get $E_{\pm}\left(x, z, t+\delta t\right)$.

4 By using staggered grid for the population inversion (see the appendix of [30] for instance), the carrier equations eqs. (2-3) are treated as in [28]. Here, the effect of carrier diffusion is not critical and can be treated classically using finite centered difference in space.

In a normal Fourier based TWM, one must use an identical temporal and longitudinal increment (the speed of light being scaled to unity), i.e. $h = \delta t$ in order to fulfill the CFL condition [23]. The DAE approach allows to decouple the two values and to "leapfrog" between spatial points, hence the idea of mesh decimation. Such a decoupling is relevant since the temporal increment must be chosen according to the stiffness of the active material response, $\gamma\delta t \ll 1$ in our case, while the spatial increment is related to the gain amplification and to the field non uniformity along the characteristics. By analogy with a TWM approach, we define the decimation factor D denoting the number of skipped spatial points as $D = h/\delta t$. When $D = 1$, one recovers the usual TWM, see [1] for details.

2.3 Reconstruction

In the case of a large decimation factor the effective mesh along the laser cavity is only composed of a few points. Still, all the complexity of the dynamics remains intact and is hidden in the past values of the field kept at each mesh point. For instance, it is still possible to reconstruct the full two dimensional profile by using the past values of the fields. Such a reconstruction at a point z_i is done from a past value t_p of the closest point on the left z_l (resp. right z_r) for the forward (resp. backward) propagating wave and reads

$$\tilde{E}\left(x, z_i, t\right) = \mathcal{F}\left\{\left[E_{\pm}\left(q, z_{l,r}, t_p\right) + t_p P_{\pm}\left(q, z_{l,r}, t_p\right)\right] e^{-\left(i\Delta q^2 + \alpha_i\right)t_p}\right\}, \tag{19}$$

with $t_p = |z_i - z_{l,r}|$. This spatial reconstruction of the longitudinal profiles of the fields achieved in eq. (19) is simply an Euler prediction from the past values to recover the corresponding mesh points. The result of such a reconstruction is exemplified in Fig. 1 in the case of a straight,

$100\,\mu$m wide BALD operated in a chaotic regime and where the dynamics is both multimode in the longitudinal and in the transverse dimension. The smoothness of the reconstructed profiles indicate a posteriori that no significant information is lost.

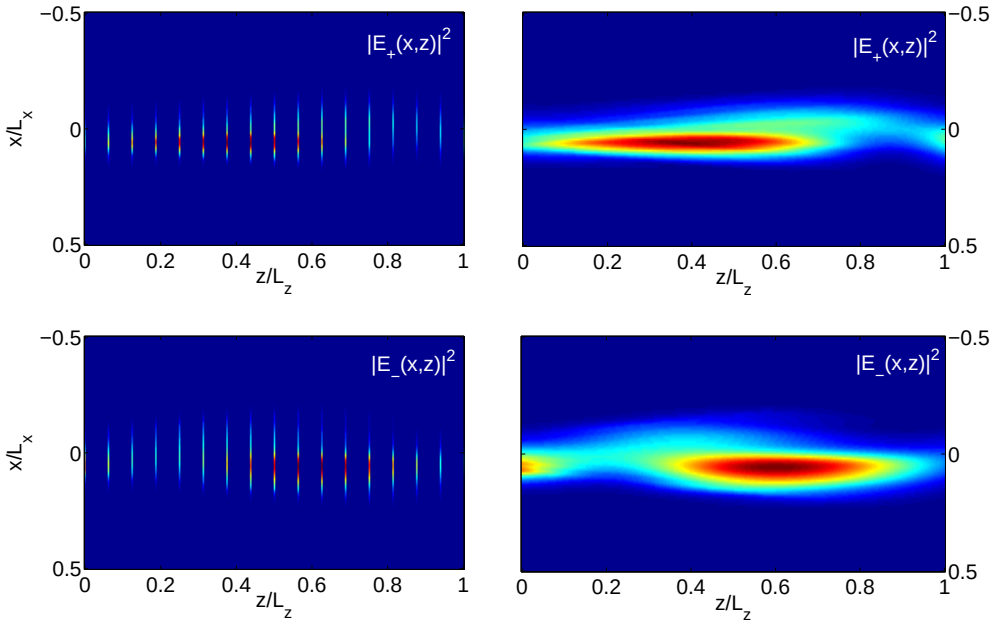

Figure 1: Mesh reconstruction from the past values in the case of a $100\,\mu$m device. The decimation factor is $D = 16$ which corresponds to $(N_z - 1)/D = 17$ points. The current is $J = 3J_{th}$ and the facet reflectivies are $r_l = 1$ and $r_r = \sqrt{0.5}$.

3 Results

In order to test the numerical method described in the previous section, we consider two BALDs of width $W_x = 28\,\mu$m and $W_x = 57\,\mu$m, as well as a wide tapered device whose transverse length ranges from $10\,\mu$m to $100\,\mu$m. We take the lateral extent of the integration region as $L_x = 2W_x$ to ensure that the fields experiencing diffraction on each side of the current stripe have a sufficient interaction length to decay smoothly to zero. Such a precaution is important since the Fourier method we use dictates periodic boundary conditions in the transverse dimension: any energy flowing out on each side is not lost and re-enters on the other side of the integration domain which may spoil the asymptotic dynamics. We assume typical values for the semiconductor material as detailed in Table 1. In addition, we fixed the mesh size to be $(N_x, N_z) = (128, 257)$. Such a convenient value of the mesh size in the longitudinal direction allows us to use decimation factors of $D = (128, 64, 32, 16, 8, 4, 2, 1)$. The longitudinal length of all devices is fixed of 1 mm which lead to a single trip of $\tau_c = 12.5$ ps and to a modal separation of 40 GHz. The temporal increment is $\delta t = \tau_c/N_z \sim 48$ fs.

Symbol	Value	Units	Meaning
λ_0	1.55	μm	Emission wavelength
n	3.75	-	Effective index
Γ	5%	-	Optical confinement factor
r	$1/0.5/0.01$	-	Facet power reflectivity
τ_c	12.5	ps	Cavity transit time
$2\alpha_i$	15	cm^{-1}	Internal losses
Ω_g	0	GHz	Band-Edge Frequency
$2\chi_0$	1500	cm^{-1}	Gain factor
b	∞	-	Empty band contribution
γ	8×10^{12}	s^{-1}	Polarization decay rate
N_t	1×10^{18}	cm^{-3}	Carrier Density at transparency
$\mathcal{D}$	20	cm^{2}s^{-1}	Ambipolar diffusion coefficient
A	1×10^8	s^{-1}	Non radiative recombination
B	7×10^{-10}	cm^{3}s^{-1}	Spontaneous recombination
C	1×10^{-29}	cm^{6}s^{-1}	Auger recombination

Table 1: Table of the parameters used in the simulations

3.1 Bifurcation diagram

As a first test of the decimation method in the bi-dimensional case, we examine the sequence of bifurcations in the mode profile that occur as a function of the bias current in the cases of a narrow and a moderately wide devices. In both cases, we consider devices that are relatively far from the uniform field limit since $r_l = 1$ and $r_r = 0.5$. It was shown in [1] that the higher decimation factors can be used when one is closer to the uniform limit. The threshold is attained for $J \sim 35$.

The upper panels in Fig. 2 show the near field output of a device with a relatively narrow stripe of width $W_x = 28\,\mu$m for $D = 1$ (i.e., no decimation and thus $N_z = 257$), while the lower panels correspond to $D = 32$ and thus $N_z = 9$. The left column is a temporal zoom of the right one. In both cases, a bifurcation from emission in the fundamental transverse mode to emission into a so-called zipper state, see [31] for details, composed of two transverse modes occurs for $J \simeq 70$. The emission profile in the zipper state alternates from one side to the other of the stripe, with a frequency that decreases with current. The dynamic characteristics (profile, oscillation frequency, etc.) of the zipper state are the same for the two cases, evidencing that decimation factors $D = 32$ preserve the dynamics of the system in the present case.

We repeated the same analysis for a broader device, $W_x = 57\,\mu$m. Here a transition from the zipper state toward chaotic transverse dynamics occurs as detailed in Fig. 3. Although the quasi-periodic zipper regime is properly reproduced, in the simplified model with $D = 32$, the time traces look different for high current although the optical spectrum remains quantitavely identical. In a chaotic regime such a discrepancy has to be expected and two times traces without decimation, i.e. $D = 1$, but with different initial conditions would look as dissimilar.

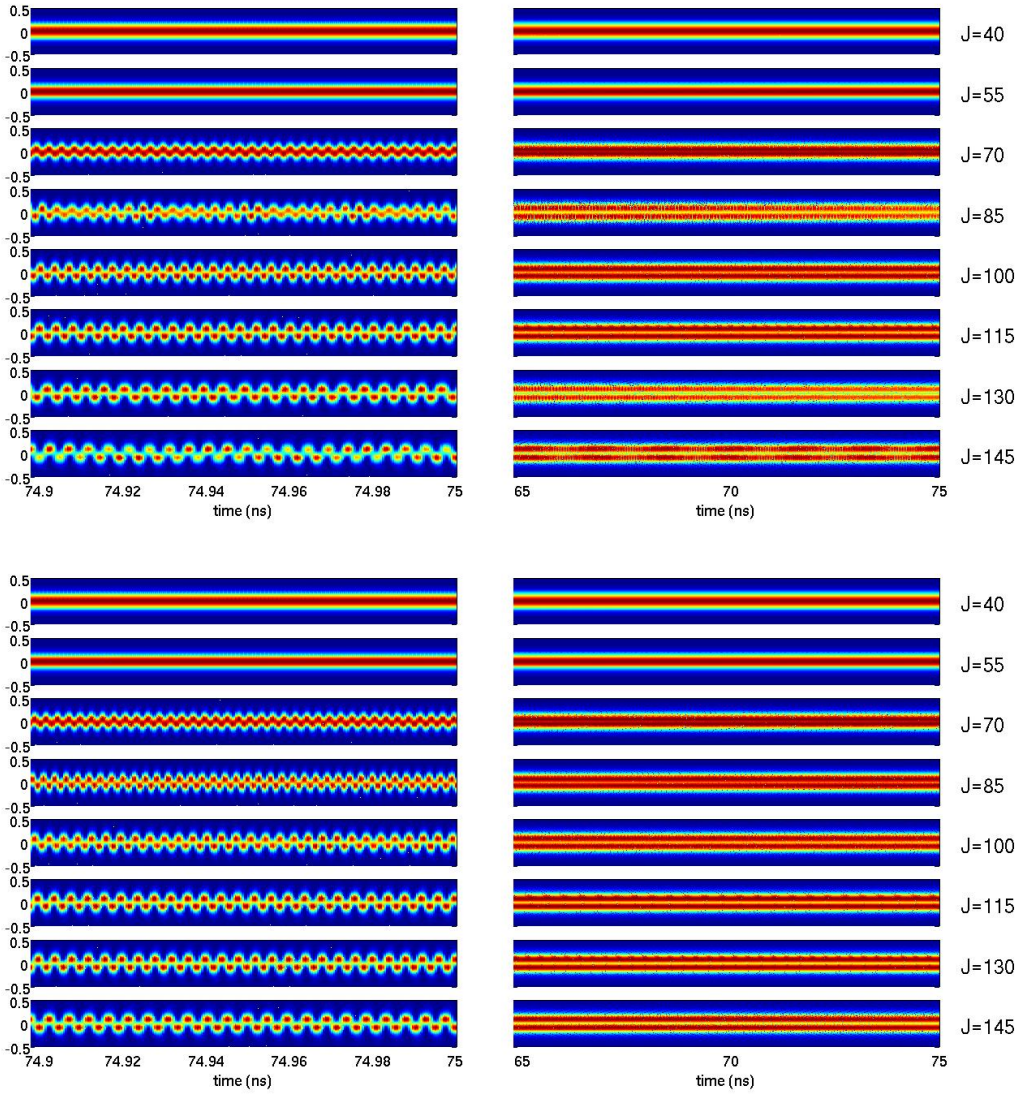

Figure 2: Numerical bifurcation diagram in the case of a $28\,\mu$m wide BALD. A zipper state emerge and remains stable up to four times threhold. The period of the zipper increases with current as expected. Excellent agreement between the full 2d TWM approach (top) and the decimated mesh approach (bottom) with $D = 32$ is found.

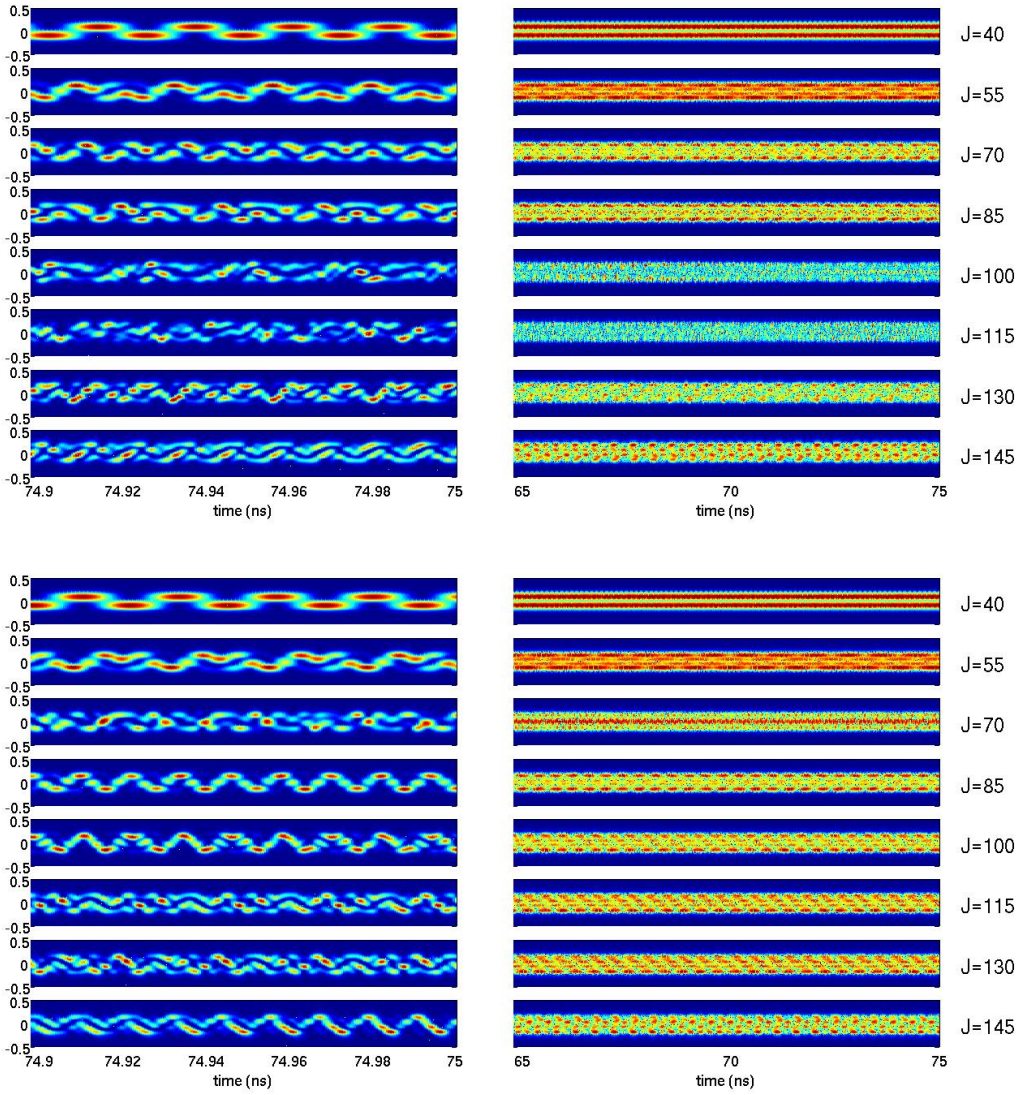

Figure 3: Numerical bifurcation diagram in the case of a $57\,\mu$m wide BALD. A zipper state emerges but do not remain stable and a transition to transverse multimode dynamics occurs. Only a qualitative agreement between the time traces of the full 2d TWM approach (top) and the decimated mesh approach (bottom) with $D = 32$ is found due to the chaotic dynamics.

3.2 Convergence test

Since it is somewhat difficult to compare chaotic time traces, we devised another test. In the case of a $57\ \mu$m wide device a full 2d TWM simulation (i.e. $D = 1$) is performed. Then, the final state of such a simulation serves as an initial condition in a second run (without any stochastic compoent) using different level of decimation, i.e. removing more and more active points from the initial condition. One expect that the chaotic trajectories remain arbitrarily close during a finite time of integration. We choose a long simulation time of $T = 1.25$ ns. The result of this approach is depicted in Fig. 4. An excellent agreement is found even after a relatively long time of integration with D up to 32. For $D = 64$ a very similar regime is found although the period is slightly affected (two extra oscillations after $T = 1.25$ ns, i.e. a 4% mismatch in the fundamental period of the quasiperiodic regime). Since the temporal time traces looks identical, we quantified the mismatch on the output facet in Fig. 5 by representing the normalized deviation between the trajectories

$$e = \frac{\int_{-\frac{1}{2}}^{\frac{1}{2}} \left| I_+^D(x,1,T) - I_+^{D=1}(x,1,T) \right| dx}{\int_{-\frac{1}{2}}^{\frac{1}{2}} I_+^{D=1}(x,1,T)\, dx}$$

In Fig. 5, we also depicted the best fit of $e(D,T)$ with a quadratic law in D thus confirming the our method is consistently of second order both in space and in time.

3.3 Tapered dynamics

We have showed so far that the decimation method discussed in [1] can be extended successfully to broad area lasers that do not operate too far from the uniform field limit (i.e. for moderate or high values of $r_l r_r$). The method also assumes implicitly a certain uniformity of the parameters in the longitudinal direction which justifies the quasi-linear approximation of the source term in eq. (16) along the forward and backward characteristics. Here we demonstrate that the method is still applicable although to a lesser extend in the most unfavorable case of a spatially dependent tapered gain medium enclosed in a strongly asymmetric cavity composed of a high reflection coated mirror and of an anti-reflection coated facet (hence low values of $r_l r_r$). The tapered gain section is linearly increased from $l_1 = 10\ \mu$m to $l_2 = 100\ \mu$m which represents an opening angle $\theta = 2.5^o$ in our 1 mm device. We assume that $r_l = 1$ and $r_r = 0.1$. The threshold current is $J_{th} = 125$. We biased the device up to $J = 1.4 J_{th}$ which is quite far from threshold for such kind of device. For all current values, the dynamics remains quantitatively identical for decimation factors up to $D = 16$ and upon increasing the bias current the near field pattern shows some amount of symmetry breaking. However, simulations performed with $D = 32$ or $D = 64$ gives erroneous predictions in the form of a self pulsating instability at the frequency of the relaxation oscillations (~ 3 GHz) for $J = 1.4 J_{th}$ as depicted in Fig. 6. Although such a bifurcation is expected after a symmetry breaking since the field is going to see more and more the umpumped regions which act as a weak saturable absorber, the bifurcation point of such a regime here is poorly estimated.

We represented in Fig. 6 a short segment of the temporal evolution of the near field pattern

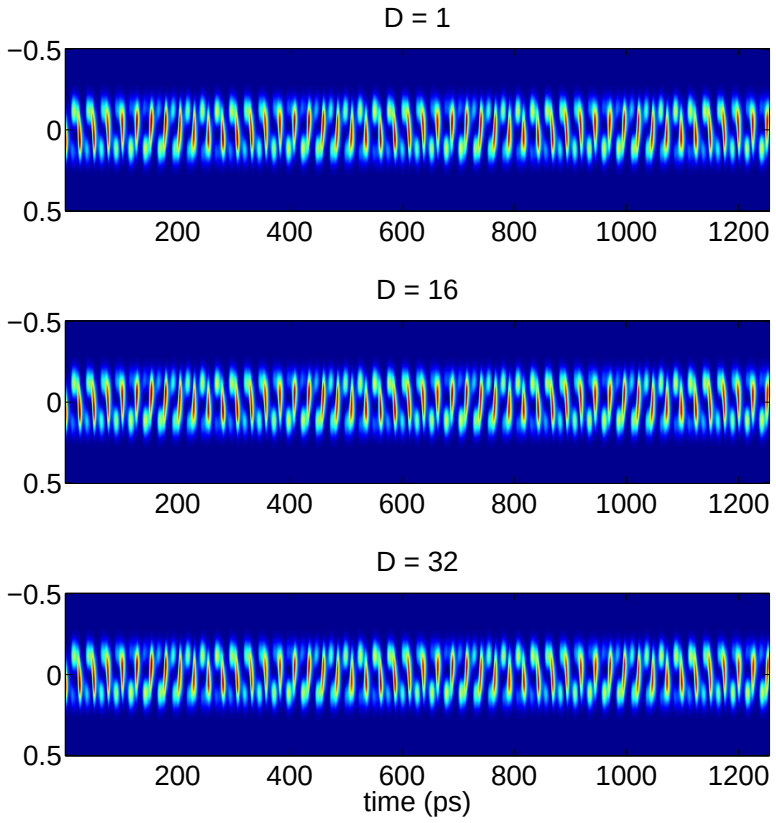

Figure 4: Spatially resolved time trace for the right output $|E_+(x,1,t)|^2$ from the same initial condition in the absence of noise and using different decimation factors. From top to bottom the decimation factors are $D = 1, 16$ and 32. An excellent agreement between the full 2d TWM approach ($D = 1$) up to $D = 32$ is found even after a long 1.25 ns integration time.

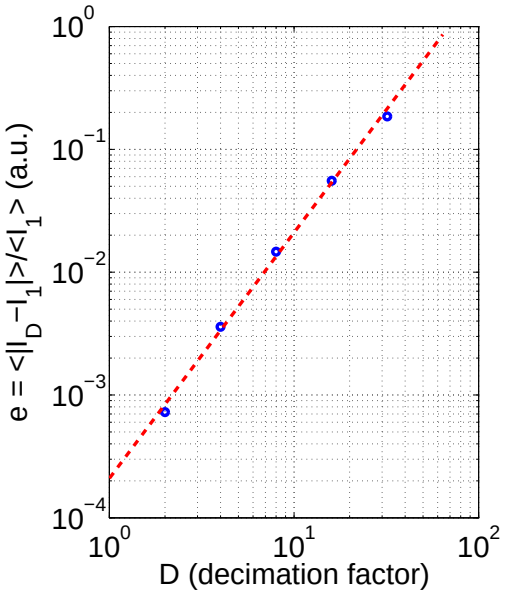

Figure 5: Error e in the near field output intensity pattern integrated over the transverse dimension on the right facet for different decimation factors. The mismatch fits with a second order law in D and remains bounded even after 1.25 ns of time integration in a chaotic regime.

as well as the beam profile on the anti-reflection coated right facet both in the case of a fully spatially resolved two dimensional TWM, i.e. $D = 1$ and with $D = 16$. The current is biased from threshold $J_{th} = 130$ toward $J = 1.5J_{th}$ where the tapered BALD develop a longitudinal multimode instability. Here again a quantitative agreement is found and the mesh reconstruction gives a smooth spatial profile. However, with $D = 32$ the multimode instability develops for lower values of the bias current and the mesh reconstruction is not smooth, which signal that the distance between spatial point is too large to perform a quasi-linear approximation in eq. (16). We exemplify in Fig.7 the mesh reconstruction with a method similar as the one discussed in Fig.1. One can clearly see that $D = 64$ is way too large and that the field reconstruction is not smooth. Some remaining artefacts can still be seen with $D = 16$ which signal that for such a demanding, tapered, asymmetric device $D = 16$ is the upper limit one can use.

3.4 CPU time

The result comes here at no surprise: the CPU time is simply divided by the decimation factor. Notice however that the memory footprint remains unaffected by the decimation factor since the “missing” spatial points are now folded into the additional time delays. The scaling of the CPU time as a function of D is depicted in Fig. 8. The typical reduction of at least one order of magnitude observed renders BALDs simulations doable on a single computer and thus avoid all the implementation difficulties associated with truly parallel MPI codes. Still, such a simplified model as the one discussed here can benefit from a moderate amount of trivial parallelism using OpenMP by sharing the longitudinal “slices” between a few cores of a multi-core processor. Here a quasi linear scaling was observed up to four cores.

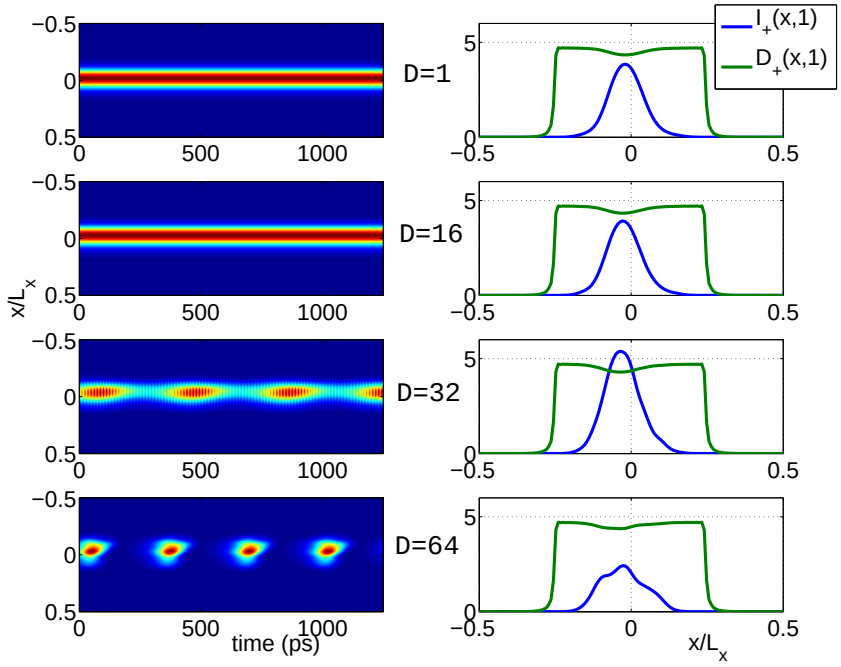

Figure 6: Time dependent near field pattern (left) and snapshot of the field intensity and carrier profiles for different decimation factors. A self pulsating regime develops due to the poor accuracy of the model for $D > 16$.

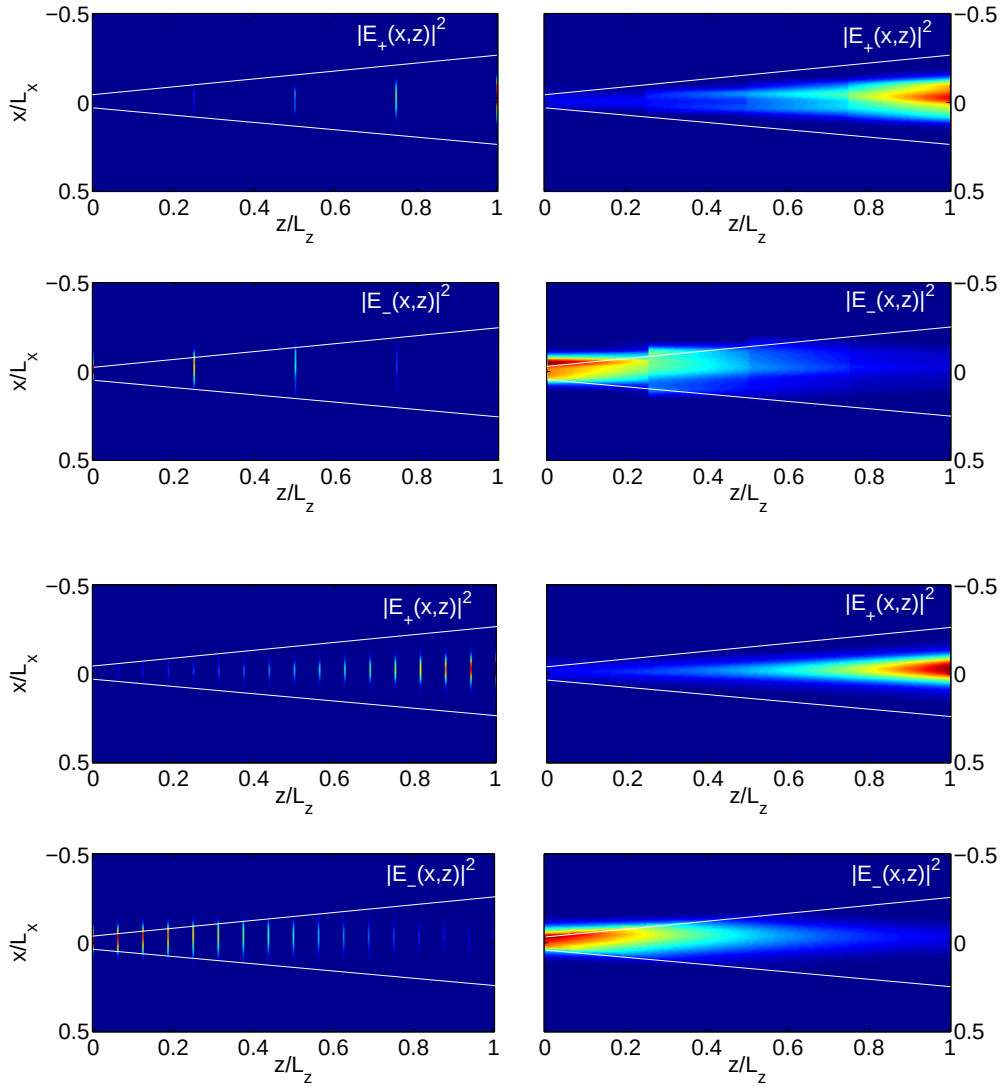

Figure 7: Mesh reconstruction from the past values in the case of a tapered device. The decimation factors are $D = 64$ and $D = 16$ from top to bottom which corresponds to $(N_z - 1)/D = 5$ and 17 points, respectively. The current is $J = 1.4 J_{th}$ and the facet reflectivies are $r_l = 1$ and $r_r = 0.1$. Notice the symmetry breaking with respect to the current stripe.

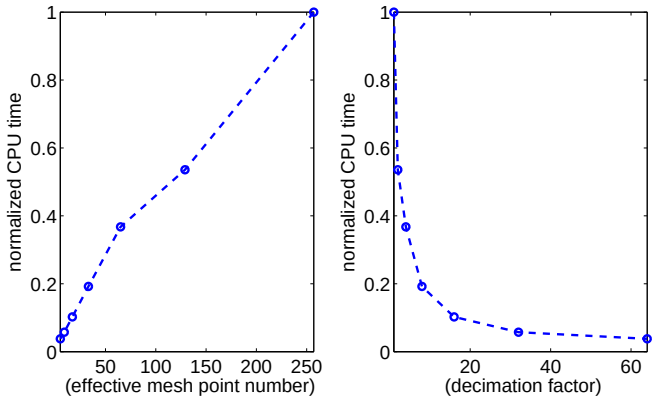

Figure 8: Normalized CPU run time for a 100 roundtrip simulation as a function of the effective number of active spatial point in the longitudinal direction $(N_z - 1)/D$ (left) and as a function of the decimation factor (right). An almost perfect linear scaling with D^{-1} is obtained.

4 Conclusion

In this manuscript we discussed how an efficient numerical approach for the simulation of BALDs based on solving the paraxial wave equations for the forward and backward-traveling waves in the spectral domain can be obtained. This allowed us to extend the idea of mesh decimation discussed in [1] to several dimensions and to the influence of diffractive terms. Such a method allows to decouple the longitudinal discretization over which the evolution is smooth and the temporal and transverse ones. The model discussed in this manuscript is based on a Padé approximation of the response of the active medium similar to the one discussed in [28]. However, Padé approximant have a restricted domain of validity in the frequency domain and are not adapted to broad band dynamics induced by e.g. reverse bias saturable absorbers. Our approach can be readily extended to other descriptions of the active medium and for instance to the time domain convolution kernel recently developed in [32, 27]. Another important improvement of the method discussed would consider the inclusion of the thermal and electro-thermal effects due to current injection and field two photon absorption which are known to play a dominant role in the dynamics of BALDs. Last but not least, distributed feedback in the weak coupling approximation and assuming uniformity of the coupling in the transverse plane can by readily implemented as in [24]. While the implementation of the aforementioned points are quite straightforwards, combining the DAE method, valid for gain guided BALD with the effect of an index guiding structure in the transverse plane remains a completely open problem.

References

[1] J. Javaloyes and S. Balle, “Multimode dynamics in bidirectional laser cavities by folding space into time delay,” *Opt. Express*, vol. 20, no. 8, pp. 8496–8502, Apr 2012. [Online]. Available: http://www.opticsexpress.org/abstract.cfm?URI=oe-20-8-8496

[2] P. Crump, S. Böldicke, C. Schultz, H. Ekhteraei, H. Wenzel, and G. Erbert, "Experimental and theoretical analysis of the dominant lateral waveguiding mechanism in 975 nm high power broad area diode lasers," *Semicond. Sci. Technol.*, vol. 27, p. 045001, 2012.

[3] J. Leidner and J. Marciante, "Beam quality improvement in broad-area semiconductor lasers via evanescent spatial filtering," *IEEE J. Quantum Electron.*, vol. 4, pp. 1269–1274, 2012.

[4] J. Gilly, P. Friedmann, H. Kissel, J. Biesenbach, and M. T. Kelemen, "High-power broad-area diode lasers optimized for fiber laser pumping," *Proc. SPIE 8241*, vol. High-Power Diode Laser Technology and Applications X, 82410T, pp. 82 410T–82 410T–6, 2012. [Online]. Available: http://dx.doi.org/10.1117/12.906701

[5] G. H. B. Thompson, "A theory for filamentation in semiconductor lasers including the dependence of dielectric constant on injected carrier density," *Opto-electronics*, vol. 4, pp. 257–310, 1972.

[6] C. M. Schultz, P. Crump, H. Wenzel, O. Brox, A. Maassdorf, G. Erbert, and G. Trankle, "11 W broad area 976 nm DFB lasers with 58 % power conversion efficiency," *Electron. Lett.*, vol. 46, pp. 580–581, 2010.

[7] R. Lang, K. Dzurko, A. Hardy, S. Demars, and A. Schoenfelder, "Theory of grating-confined broad-area lasers," *IEEE J. Quantum Electron.*, vol. 34, pp. 2196–2210, 1998.

[8] K. Paschke, R. Güther, J. Fricke, F. Bugge, G. Erbert, and G. Tränkle, "High power and high spectral brightness in 1060 nm α-DFB lasers with long resonators," *Electron. Lett.*, vol. 39, pp. 269–270, 2003.

[9] H. Adachihara, O. Hess, E. Abraham, P. Ru, and P. Moloney, "Spatiotemporal chaos in broad-area semiconductor lasers," *J. Opt. Soc. Am. B*, vol. 10, pp. 658–665, 1993.

[10] W. Chow and H. Amano, "Analysis of lateral-mode behavior in broad-area InGaN quantum-well lasers," *IEEE J. Quantum Electron.*, vol. 37, pp. 265–273, 2001.

[11] J. Martín-Regalado, G. H. M. van Tartwijk, S. Balle, and M. San Miguel, "Mode control and pattern stabilization in broad-area lasers by optical feedback," *Phys. Rev. A*, vol. 54, p. 5386, 1996.

[12] S. K. Mandre, I. Fischer, and W. Elsässer, "Spatiotemporal emission dynamics of a broad-area semiconductor laser in an external cavity: stabilization and feedback-induced instabilities," *Opt. Comm.*, vol. 244, pp. 355–365, 2005.

[13] H. Odriozola, J. Tijero, L. Borruel, I. Esquivias, H. Wenzel, F. Dittmar, K. Paschke, B. Sumpf, and G. Ebert, "Beam properties of 980-nm tapered lasers with separate contacts: Experiments and simulations," *IEEE J. Quantum Electron.*, vol. 45, no. 1, pp. 42–50, 2009.

[14] M. Spreemann, M. Lichtner, M. Radziunas, U. Bandelow, and H. Wenzel, "Measurement and simulation of distributed-feedback tapered master-oscillators power-amplifiers," *IEEE J. Quantum Electron.*, vol. 45, pp. 609–616, 2009.

[15] C. Chen, P. Leisher, S. Patterson, P. Crump, Y. K. Kim, and K. Choquette, "Stabilization of lateral mode transients in high-power broad-area semiconductor lasers," *Appl. Phys. Lett.*, vol. 94, p. 011107, 2009.

[16] U. Bandelow, H. Gajewski, and R. Hünlich, *Optoelectronics Devices - Advanced Simulation and Analysis*. Springer, New York, 2005, ch. "Fabry-Perot lasers: Thermodynamics based modeling", pp. 63–85.

[17] A. E. Siegman, "Laser beams and resonators: The 1960s," *IEEE J. Sel. Top. Quantum Electron.*, vol. 6, pp. 1380–1388, 2000.

[18] J. J. Lim, T. M. Benson, and E. C. Larkins, "Design of wide-emitter single-mode laser diodes," *IEEE J. Quantum Electron.*, pp. 506–516, 2005.

[19] R. Lang, A. Larsson, and J. Cody, "Lateral modes of broad area semiconductor lasers: theory and experiment," *IEEE J. Quantum Electron.*, vol. 27, pp. 312–320, 1991.

[20] S. Blaaberg, P. Petersen, and B. Tromborg, "Structure, stability, and spectra of lateral modes of a broad-area semiconductor laser," *IEEE J. Quantum Electron.*, vol. 43, pp. 959–973, 2007.

[21] H. Adachihara, O. Hess, R. Indik, and P. V. Moloney, "Semiconductor laser array dynamics: numerical simulations and multistripe index-guided lasers," *J. Opt. Soc. Am. B*, vol. 10, pp. 496–506, 1993.

[22] K. Böhringer and O. Hess, "A full-time-domain approach to spatio-temporal dynamics of semiconductor lasers. I. Theoretical formulation," *Progress in Quantum Electronics*, vol. 32, no. 5-6, pp. 159 – 246, 2008. [Online]. Available: http://www.sciencedirect.com/science/article/B6TJD-4TTHW8B-1/2/056e436695dc287b520d0935da6e7b97

[23] R. Courant, K. Friedrichs, and H. Lewy, "Über die partiellen differenzengleichungen der mathematischen physik," *Mathematische Annalen*, vol. 100, no. 1, pp. 32–74, 1928.

[24] J. Javaloyes and S. Balle, "Freetwm: a simulation tool for multisection semiconductor lasers," 2012. [Online]. Available: http://nova.uib.es/ONL/Softwares/Softwares.html

[25] S. Balle, "Analytical description of spectral hole-burning effects in active semiconductors," *Opt. Lett.*, vol. 21, pp. 1923–1925, 2002.

[26] ——, "Simple analytical approximations for the gain and refractive index spectra in quantum well lasers," *Phys. Rev. A*, vol. 57, pp. 1304–1312, 1998.

[27] J. Javaloyes and S. Balle, "Quasiequilibrium time-domain susceptibility of semiconductor quantum wells," *Phys. Rev. A*, vol. 81, no. 6, p. 062505, Jun 2010.

[28] ——, "Emission directionality of semiconductor ring lasers: A traveling-wave description," *Quantum Electronics, IEEE Journal of*, vol. 45, no. 5, pp. 431–438, May 2009.

[29] J. A. Fleck, "Ultrashort-pulse generation by Q-switched lasers," *Phys. Rev. B*, vol. 1, no. 1, p. 84, Jan 1970.

[30] A. Pérez-Serrano, J. Javaloyes, and S. Balle, "Bichromatic emission and multimode dynamics in bidirectional ring lasers," *Phys. Rev. A*, vol. 81, no. 4, p. 043817, Apr 2010.

[31] I. Fischer, O. Hess, W. Elsässer, and E. Göbel, "Complex spatio-temporal dynamics in the near-field of a broad-area semiconductor laser," *Europhys. Lett.*, vol. 35, pp. 579–584, 1996.

[32] J. Javaloyes and S. Balle, "Detuning and thermal effects on the dynamics of passively mode-locked quantum-well lasers," *Quantum Electronics, IEEE Journal of*, vol. 48, pp. 1519-1526, Dec 2012.